

Influence of the Fermi surface geometry on a Josephson effect between an iron-pnictide and conventional superconductors

A. A. Kalenyuk^{1,2}, E. A. Borodianskyi¹, A. A. Kordyuk^{2,3}, and V. M. Krasnov^{1,4*}

¹Department of Physics, Stockholm University, AlbaNova University Center, SE-10691 Stockholm, Sweden;

²Institute of Metal Physics of National Academy of Sciences of Ukraine, 03142 Kyiv, Ukraine;

³Kyiv Academic University, 03142 Kyiv, Ukraine; and

⁴Moscow Institute of Physics and Technology, State University, 141700 Dolgoprudny Russia.

We study Josephson junctions between a multi-band iron-pnictide $\text{Ba}_{1-x}\text{Na}_x\text{Fe}_2\text{As}_2$ and conventional s -wave superconductors Nb and Cu/Nb bilayer. We observe that junctions with a Cu interlayer exhibit much larger $I_c R_n$, despite a weaker proximity-induced superconductivity. This counterintuitive result is attributed to the difference in Fermi surface geometries of Nb and Cu, which leads to a selective one-band tunneling from Cu and a non-selective multi-band tunneling from Nb. The latter leads to a mutual cancellation of supercurrents due to the sign-reversal s_{\pm} symmetry of the order parameter in the pnictide. Our results indicate that Fermi surface geometries play a crucial role for pnictide-based junctions. This provides a new tool for phase sensitive studies and paves a way to a conscious engineering of such junctions.

Electronic structure of superconductors is usually quite complicated, even for low- T_c materials, such as the transition metal Nb. Nevertheless, a simple description of Josephson effects, which does not take into account complex Fermi surface (FS) geometry, works remarkably well for conventional superconductors [1, 2]. This happens because probabilities of electron and Cooper-pair tunneling are similar [3]. Together with a momentum-independent s -wave energy gap, Δ , it leads to the inverse relationship between the normal resistance, R_n , and the critical current, I_c . Thus, the $I_c R_n$ product becomes a universal function of Δ , independent of FS geometry [4].

This universality, however, breaks for unconventional multi-band superconductors. A particularly drastic deviation should occur in the case of sign-reversal order parameter [5–8]. This occurs in cuprate and iron-based superconductors, which are believed to have d -wave [9, 10] and s_{\pm} [11–14] symmetries, respectively. In this case, I_c depends on gap values in each band, and the $I_c R_n$ is band-structure-sensitive and not universal [5–8, 15].

In this work we fabricate and study high-quality Josephson junctions (JJ's) between single crystals of an iron-pnictide $\text{Ba}_{1-x}\text{Na}_x\text{Fe}_2\text{As}_2$ (BNFA) and conventional low- T_c superconductors made of either Nb film or Cu/Nb bilayer. Both types of JJ's exhibit clean and clear Josephson phenomena. However, JJ's with a Cu interlayer exhibit almost two order of magnitude larger $I_c R_n$, despite a weaker proximity-induced superconductivity in Cu. This counterintuitive result is attributed to the difference in FS geometries of Nb [multiple FS's at various parts of the Brillouin zone (BZ)] and Cu [a single quasi-spherical FS]. Therefore, tunneling from Nb takes place into all bands of BNFA. Due to the sign-reversal s_{\pm} order parameter in BNFA, this leads to a mutual cancellation of supercurrents and a very small $I_c R_n \sim 3\mu\text{V}$. To the contrary, tunneling from Cu occurs predominantly into one sub-band avoiding such cancellation and leading to a significantly larger $I_c R_n \simeq 200\mu\text{V}$. Our results indi-

cate that FS geometries play a crucial role for JJ's with multi-band, sign-reversal superconductors. This provides a new tool for fundamental studies of unconventional superconductivity and opens a possibility for optimization and adjustment of junction characteristics.

Figure 1 (a) represents a scanning electron microscope (SEM) image of the BNFA-Cu/Nb sample. Our samples contain six junctions made on a freshly cleaved BNFA single crystal. Fig. 1 (b) shows a closeup on the junction. Here the vertical strip represents the window in SiO_2 isolation layer and the horizontal strip - the top contact electrode. Micrometer-size JJ's are formed at the overlap between the two strips. As the top electrode we use either pure Nb film (~ 200 nm thick) or Cu(15 nm)/Nb(180 nm) bilayer deposited by magnetron sputtering in a single cycle without breaking vacuum. Details of sample fabrication, experimental setup and a list of JJ parameters can be found in the Supplementary [15].

Multiterminal configuration of our samples allows simultaneous measurements of junction and crystal characteristics [23, 24]. The blue line in Fig. 1 (c) shows the in-plane resistive transition of BNFA. At $T \sim 150$ K there is a kink in $R(T)$, corresponding to a structural transition and spin-density-wave (SDW) ordering [12, 14]. The superconducting transition occurs at $T_c(\text{BNFA}) \simeq 30$ K. Observation of the SDW state and the slightly sub-optimal T_c indicate that the BNFA crystal is moderately underdoped. The red line in Fig. 1 (c) shows a simultaneously measured resistive transition of a junction. It has two steps, first at $T_c(\text{BNFA})$ and the second at $T_c(\text{Nb}) \sim 9$ K.

Figs. 1 (d) and (e) show current-voltage (I - V) characteristics at different T for (d) BNFA-Nb and (e) BNFA-Cu/Nb JJ's. In both cases the I - V 's have the shape typical for resistively shunted JJ's [1, 2] with a well defined I_c and R_n . Green, blue and red curves are measured at zero field. The wine-color line in Fig. 1 (d) shows the I - V at $T \simeq 0.3$ K, measured at in-plane magnetic field of

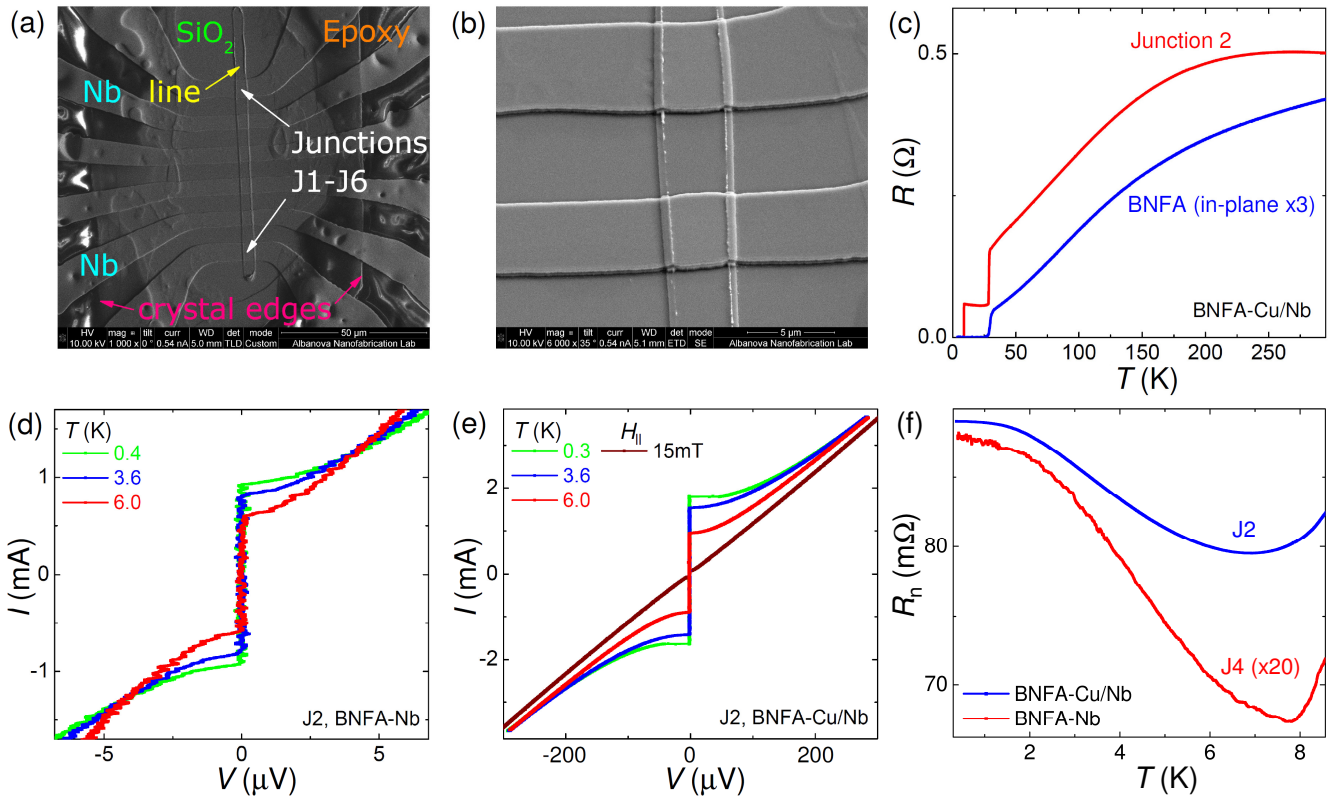


FIG. 1. (Color online). (a) and (b) SEM images of the BNFA-Cu/Nb sample. The sample contains six junctions J1-6 (a), formed at a cross-like overlap between a window in the insulation SiO_2 layer and top electrodes (b). (c) Resistive transitions of a junction (J2, red) and BNFA crystal (blue) for the BNFA-Cu/Nb sample. (d) and (e) I - V curves at different temperatures and $H = 0$ for junctions at (d) BNFA-Nb and (e) BNFA-Cu/Nb samples. The wine curve in (d) represents I - V at $T \simeq 0.3$ K and $H_{\parallel} = 15$ mT. It demonstrates a complete suppression of I_c by a modest in-plane magnetic field. (f) Temperature dependencies of normal resistances for BNFA-Nb (red) and BNFA-Cu/Nb (blue) junctions.

$B_{\parallel} = 15$ mT. It is seen that I_c is completely suppressed by a small parallel field, much smaller than the upper critical fields of BNFA [23, 25] and Nb [26]. Therefore, in such a field we can carefully measure temperature dependence $R_n(T)$, as shown in Fig. 1 (f). The modest upturn of R_n with decreasing T is quite common for c -axis characteristics of high- T_c superconductors, commonly associated with a pseudogap [27].

Suppression of I_c by small parallel field is caused by flux quantization in the junction. Figure 2 (a) shows $I_c(H_{\parallel})$ modulations at different temperatures for a BNFA-Cu/Nb JJ. Fig. 2 (b) represents normalized $I_c/I_c(0)$ versus flux curves for BNFA-Nb (blue) and BNFA-Cu/Nb (red) JJ's at low T . Both types of JJ's exhibit clear Fraunhofer modulation depicted by the black line. This is a figure of merit indicating good uniformity of JJ's [1, 2].

Figure 2 (c) shows I - V curves of a BNFA-Cu/Nb JJ without (black) and with (red) applied high-frequency electromagnetic radiation at $f \simeq 74$ GHz at $H = 0$ and $T \simeq 0.4$ K. A clear Shapiro step is seen at $V_1 = hf/2e$. Fig. 2 (d) shows the normalized differential conductance for this I - V as a function of V_1/V . It reveals nu-

merous subharmonic Shapiro steps. This indicates the strongly non-sinusoidal current-phase relation in the JJ [28], which is indeed anticipated for s - s_{\pm} JJ's [7, 8]. On the other hand, the non-sinusoidality may also be caused by the proximity effect in the Cu/Nb bilayer [29].

Thus, our JJ's exhibit clean and clear dc- and ac-Josephson effects. The high quality of the JJ's together with a good reproducibility of junction parameters (see the Supplementary [15]) allows us to investigate genuine characteristics of composing them superconductors (as opposed to interface defects). Figs. 2 (e) and (f) show temperature dependencies of (e) the critical current density J_c and (f) the $I_c R_n$ product for both types of junctions. Despite similarities in behavior, the same BNFA crystal [15] and fabrication procedure, the two types of JJ's exhibit largely (almost by two orders of magnitude) different $I_c R_n$ values. BNFA-Nb JJ's have a very small $I_c R_n \simeq 3 \mu\text{V}$ [24], much smaller than $\Delta/e > 1$ mV in both superconductors, while for BNFA-Cu/Nb JJ's $I_c R_n \simeq 200 \mu\text{V}$. The difference can be clearly seen in the I - V curves from Figs. 1 (d) and (e). The reported remarkable influence of the thin Cu interlayer is the key observation of this work.

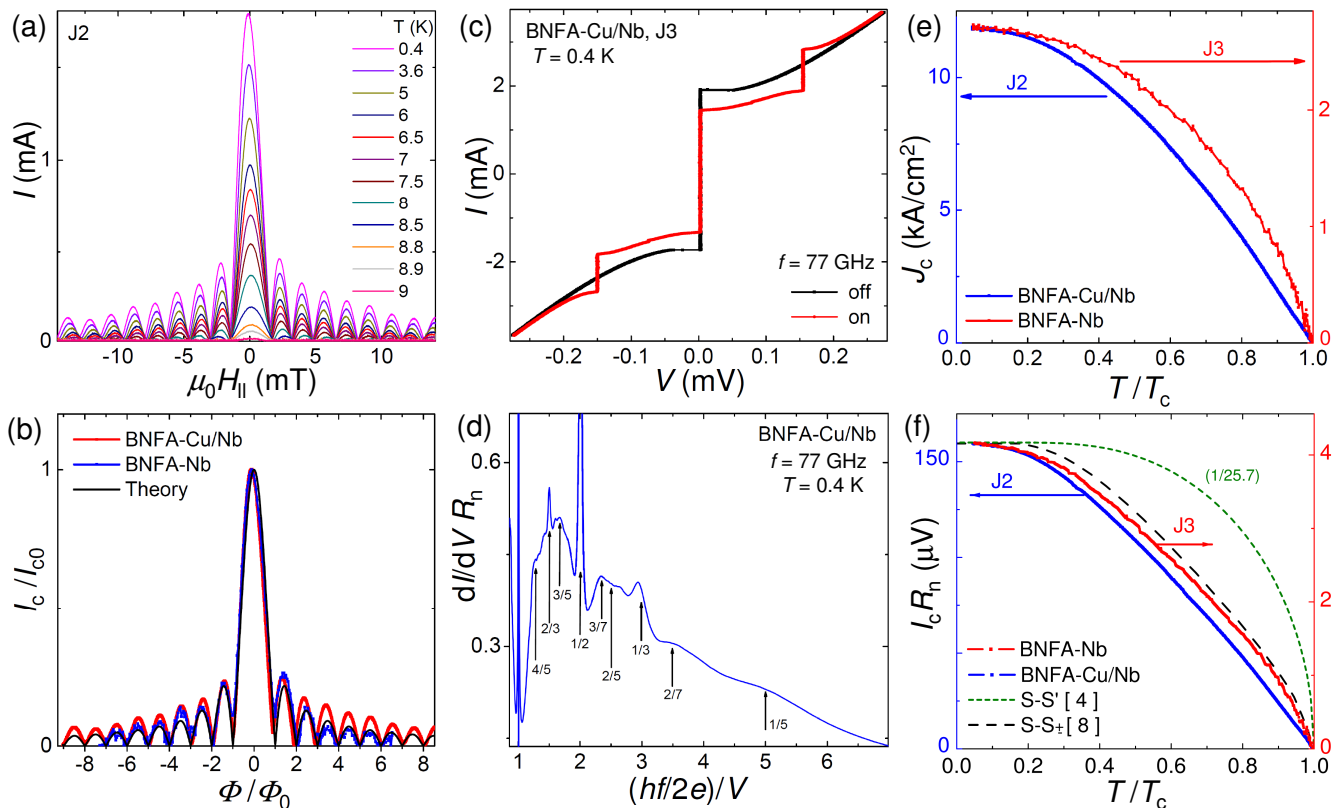


FIG. 2. (Color online). (a) Modulation of the critical current versus in-plane magnetic field for a BNFA-Cu/Nb junctions at different temperatures. (b) Comparison of I_c versus flux modulation patterns of BNFA-Cu/Nb (red), BNFA-Nb (blue) and Fraunhofer pattern (black). (c) I - V characteristics of BNFA-Cu/Nb junction with (red) and without (black) microwave radiation. The primary Shapiro step is clearly seen. (d) Differential conductance versus inverse voltage, demonstrating presence of sub-harmonic Shapiro steps. (e) Temperature dependencies of critical current densities of BNFA-Cu/Nb (blue, left scale) and BNFA-Nb (red, right scale) junctions. (f) Temperature dependencies of $I_c R_n$ products for the same junctions. Note a big difference of $I_c R_n$ values. The dotted black line represents a normalized theoretical curve for conventional s -wave superconductors [4]. The dashed black line shows a simulated dependence for an s - s_{\pm} junctions from Ref. [8].

The increase of $I_c R_n$ in BNFA-Cu/Nb JJ's is associated with the increase of R_n . The latter indicates that the interface transparency, β , between BNFA and Cu is reduced compared to BNFA-Nb. Yet, as mentioned above, this does not explain the increase of $I_c R_n$ because usually $I_c \propto 1/R_n$ and $I_c R_n$ is independent of β .

The proximity induced superconducting order parameter in Cu at the junction interface is $\Phi_N \simeq \beta \Psi_S \exp(d_N/\xi_N)$, where Ψ_S is the order parameter in Nb, $d_N = 15$ nm is the Cu layer thickness and ξ_N is the coherence length in Cu. According to Ref. [30], for thin sputtered Cu films $\xi_N \simeq 18\sqrt{T_c(Nb)/T}$ (nm), where $T_c(Nb) \simeq 9$ K. It gives $\xi_N(0.3K) \simeq 100$ nm, $\xi_N(3K) \simeq 30$ nm and $\xi_N(T_c(Nb)) \simeq 18$ nm. Thus, our Cu interlayer is always thinner than ξ_N . Although Cu and Nb films are deposited without breaking vacuum, the Cu/Nb interface transparency is modest, $\beta \simeq 0.4$ [30], predominantly due to the FS mismatch between Nb and Cu. Thus the proximity induced order parameter in Cu is smaller than in Nb. For SINS JJ's (I - insulator,

N-normal metal) made of s -wave superconductors, the proximity effect leads to the reduction of $I_c R_n$ [31]. This is opposite to our observation. This discrepancy points out that the unconventional (non- s -wave) symmetry of the order parameter in BNFA plays an essential role. In particular, the extremely small $I_c R_n$ of BNFA-Nb junctions provides evidence for the sign-reversal s_{\pm} symmetry in BNFA, due to which supercurrents from bands with opposite signs of Δ cancel each other [24].

For a more quantitative understanding we consider FS geometries of involved metals. Figures 3 (a-c) show DFT calculated three-dimensional images of Fermi surfaces for Cu (a), Nb (b) [32, 33] and BNFA (c) [34]. FS of Cu is simple quasi-spherical. The transition metal Nb has a very complex FS with many small pockets spread over the BZ. BNFA has two bunches of the FS sheets, the three large quasi-cylinders in the center and the propeller-like FS's at the corners of the BZ [35, 36]. Those bunches are believed to have opposite signs of Δ [12, 13].

Electron tunneling between two metals usually con-

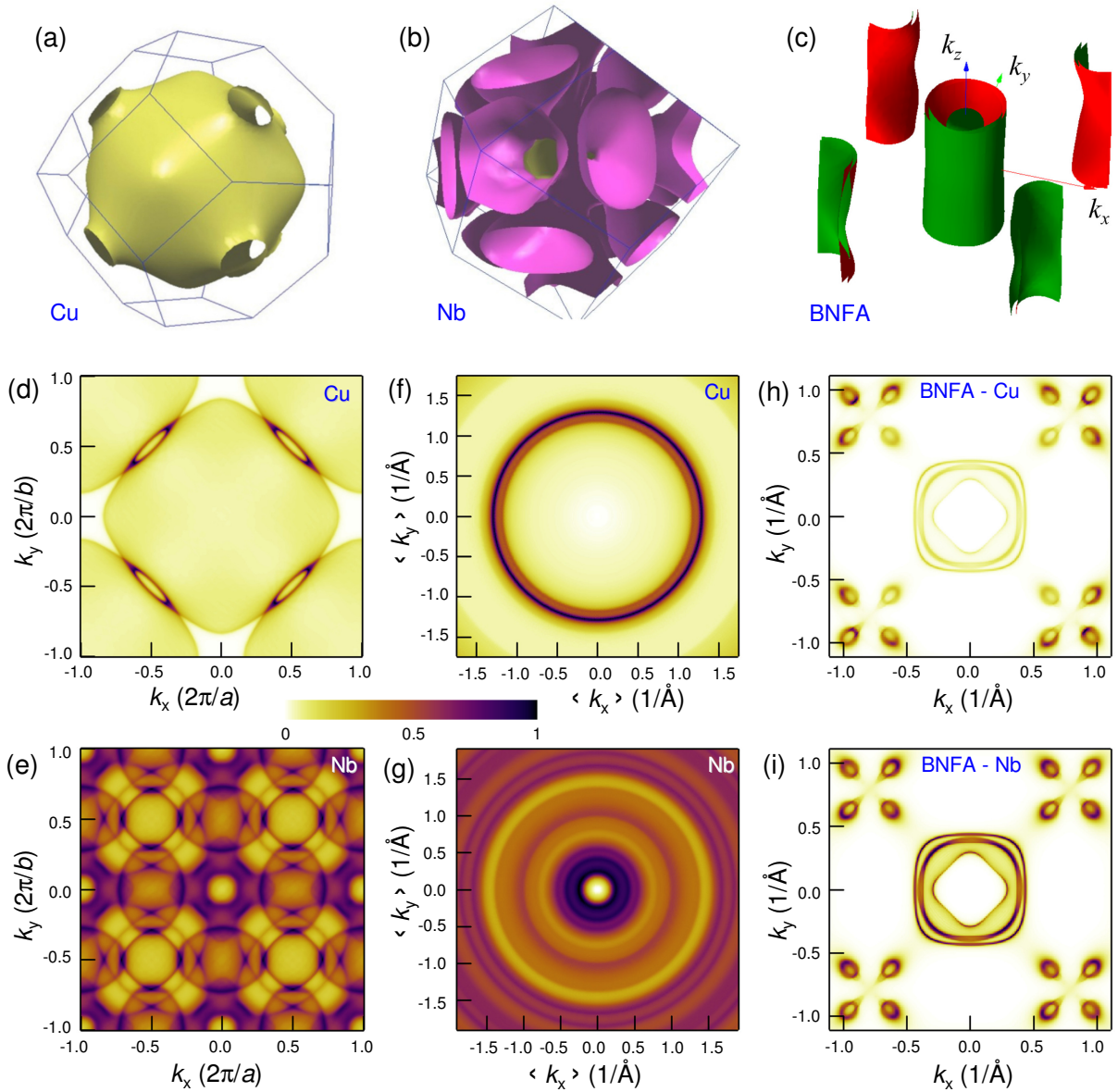


FIG. 3. (Color online). (a-c) The Fermi surface topologies in the 1st Brillouin zone for (a) Cu, (b) Nb and (c) BNFA. (d) and (e) The k_z -integrated projections of Fermi surfaces on the (001) plane for Cu (d) and Nb (e). (f) and (g) The same projections averages over the in-plane momentum angle, representing the effective (k_z -integrated) density-of-states distribution for poly-crystalline Cu (f) and Nb (g) films. (h) and (i) Product of k_z -integrated Fermi surface projection of BNFA with effective density-of-states for Cu (h) and Nb (i). It can be seen that for BNFA-Cu junctions tunneling current flows predominantly into the propeller-like corner bands of BNFA (h). On the other hand, for BNFA-Nb junctions the tunneling current is distributed relatively uniformly between central and corner bands.

serves the in-plane momentum $\mathbf{k}_{\parallel} = (k_x, k_y)$. Therefore, the total single-electron current can be written as

$$J \propto \oint T_{12}^2 A_1(k_{z1}, \mathbf{k}_{\parallel}) A_2(k_{z2}, \mathbf{k}_{\parallel}) (f_1 - f_2) dk_{\parallel} dk_{z1} dk_{z2},$$

where T_{12} is the tunneling matrix element between initial and final states, (k_{z1}, k_x, k_y) and (k_{z2}, k_x, k_y) , in the two electrodes, $A_{1,2}$ are the spectral functions (momentum-dependent density of states) and $f_{1,2}$ are the corresponding distribution functions. The key band-structure-

dependent factor is the density of states projection on the junction plane, which can be integrated independently

$$N_i(\mathbf{k}_{\parallel}) = \int A_i(k_{zi}, \mathbf{k}_{\parallel}) dk_{zi}, \quad (i = 1, 2). \quad (1)$$

Figs. 3 (d) and (e) show such projections for Cu and Nb. The corresponding projection for BNFA is pretty similar to the pattern, shown in Fig. 3 (i).

For comparison with experiment we must take into account the polycrystalline structure of Cu and Nb elec-

trodes and make an average with respect to random crystalline orientation. This is similar to averaging with respect to rotation of $k_{x,y}$ axes. Figs 3 (f) and (g) show thus averaged projections, $\langle N_i(k_x, k_y) \rangle$, for polycrystalline Cu and Nb. The key difference is that due to the quasi-spherical FS of Cu, the polycrystalline density of states projection keeps the circular shape with the radius given by the Fermi momentum. To the contrary, averaging for multi-band polycrystalline Nb leads to a more uniform distribution of the density of states.

Figs. 3 (h) and (i) show a product of the density of state projections (h) $\langle N_{Cu}(k_x, k_y) \rangle N_{BNFA}(k_x, k_y)$ for BNFA-Cu/Nb and (i) $\langle N_{Nb}(k_x, k_y) \rangle N_{BNFA}(k_x, k_y)$ for BNFA-Nb junctions. It gives a hint about contribution of the two BNFA bands in electrical current through the junction. For BNFA-Nb JJ's both BNFA bands participate approximately equally due to fairly uniform distribution of $\langle N_{Nb}(k_x, k_y) \rangle$ in the BZ projection, Fig. 3 (g). To the contrary, the highly non-uniform, circular-shape $\langle N_{Cu}(k_x, k_y) \rangle$, Fig. 3 (f), blocks tunneling into the central band of BNFA.

For calculation of supercurrent, A_i should be replaced by $A_i\Psi_i$, where Ψ_i is the superconducting order parameter in the corresponding metal. For Nb and Cu/Nb with s -wave order parameter Ψ is just a number. However, for the unconventional two-band superconductor BNFA, which likely has the s_{\pm} symmetry, Ψ changes sign between central and corner bands. For BNFA-Nb JJ's with similar transport contribution of the two bands this leads to an almost complete cancellation of the total supercurrent [24]. However, for BNFA-Cu/Nb JJ's the cancellation is much smaller because tunneling from central bands is suppressed. Therefore, such analysis qualitatively explains larger values of both R_n and $I_c R_n$ in BNFA-Cu/Nb junctions.

To conclude, we fabricated and studied high-quality Josephson junctions between an iron-pnictide superconductor $Ba_{1-x}Na_xFe_2As_2$ and either a conventional low- T_c superconductors Nb or a Cu/Nb bilayer. Remarkably, we observed that addition of a very thin (15 nm) Cu interlayer changes drastically junction properties and, in particular, increases the $I_c R_n$ product by almost two orders of magnitude. The latter is opposite to expectations for proximity-coupled junctions made of conventional s -wave superconductors [31]. This counterintuitive result adds to evidence for the unconventional s_{\pm} symmetry of the order parameter in the pnictide. The phenomenon is explained qualitatively taking into account particular Fermi surface geometries of involved metals. It is shown that the multi-band structure of Nb leads to similar contributions of both pnictide bands into electron transport, which due to the sign-reversal s_{\pm} superconducting order parameter in the two electronic bands of the pnictide, leads to the cancellation of the total supercurrent and results in a very small $I_c R_n \simeq 3 \mu V$ [24]. To the contrary, the simple quasi-spherical Fermi sur-

face of Cu supports tunneling predominantly from only one band, avoiding the supercurrent cancellation and resulting in much larger $I_c R_n \simeq 200 \mu V$. Our results indicate that unlike for junctions made of conventional s -wave superconductors, for junctions with unconventional sign-reversal superconductors the Fermi surface geometry plays a crucial role. This provides a new tool for phase sensitive studies of such materials and could probably explain some of reported variations of $I_c R_n$ values in pnictide JJ's [8, 24, 37]. The reported material-dependence of tunneling into pnictide superconductors can be used for optimization and conscious engineering of pnictide-based Josephson junctions.

The work was supported by the National Research Foundation of Ukraine (project 2020.02/0408) and the Russian Science Foundation (Grant No. 19-19-00594). The paper was accomplished during a sabbatical period of V.M.K. at MIPT. We are grateful to A.N. Yaresko for providing the results of DTF calculations, V.V. Zabolotnyy for help with FS visualization, S. Aswartham, S. Wurmehl and B. Büchner for providing BNFA crystals.

* Vladimir.Krasnov@fysik.su.se

- [1] A. Barone and C. Paterno, *Physics and Applications of the Josephson Effect* (Wiley, New York, 1982).
- [2] K. K. Likharev, *Dynamics of Josephson Junctions and Circuits* (Gordon and Breach Sc. Publ., Amsterdam, 1986).
- [3] D.G. McDonald, The Nobel laureate versus the graduate student, *Physics Today* **54**, 46 (2001).
- [4] V. Ambegaokar and A. Baratoff, Tunneling between superconductors, *Phys. Rev. Lett.* **10**, 486 (1963); *ibid.* **11**, 104 (1963).
- [5] Y. Tanaka and S. Kashiwaya, Theory of Josephson effects in anisotropic superconductors, *Phys. Rev. B* **56**, 892 (1997).
- [6] Y. Ota, M. Machida, T. Koyama, and H. Matsumoto. Theory of Heterotic Superconductor-Insulator-Superconductor Josephson Junctions between Single- and Multiple-Gap Superconductors, *Phys. Rev. Lett.* **102**, 237003 (2009).
- [7] I. B. Sperstad, J. Linder, and A. Sudbø, Quantum transport in ballistic s_{\pm} -wave superconductors with interband coupling: Conductance spectra, crossed Andreev reflection, and Josephson current, *Phys. Rev. B* **80**, 144507 (2009).
- [8] A. V. Burmistrova, I. A. Devyatov, A. A. Golubov, K. Yada, Y. Tanaka, M. Tortello, R. S. Gonnelli, V. A. Stepanov, X. Ding, H. H. Wen, and L. H. Green. Josephson current in Fe-based superconducting junctions: Theory and experiment, *Phys. Rev. B* **91**, 214501 (2015).
- [9] D. A. Wollman, D. J. Van Harlingen, W. C. Lee, D. M. Ginsberg, and A. J. Leggett, Experimental determination of the superconducting pairing state in YBCO from the phase coherence of YBCO-Pb dc SQUIDS, *Phys. Rev. Lett.* **71**, 2134 (1993).

- [10] C. C. Tsuei and J. R. Kirtley, Pairing symmetry in cuprate superconductors, *Rev. Mod. Phys.* **72**, 969 (2000).
- [11] T.K. Ng and N. Nagaosa. Broken time-reversal symmetry in Josephson junction involving two-band superconductors, *EPL* **87**, 17003 (2009).
- [12] P. J. Hirschfeld, M. M. Korshunov, and I. I. Mazin, Gap symmetry and structure of Fe-based superconductors, *Rep. Prog. Phys.* **74**, 124508 (2011).
- [13] F. Wang, D.-H. Lee, The electron-pairing mechanism of iron-based superconductors. *Science* **332**, 200 (2011).
- [14] A. Chubukov, Pairing Mechanism in Fe-Based Superconductors, *An. Rev. Cond. Matt. Phys.* **3**, 57 (2012).
- [15] See EPAPS Document No.XXX. The supplementary material provides additional information about (i) Sample fabrication, (ii) Additional transport characterization (iii) Junction parameters, and (iv) Numerical analysis of temperature dependence of $I_c R_n$ in junctions between a conventional s -wave superconductor and a two-band s_{\pm} superconductor, and includes Refs. [16–22].
- [16] V. M. Krasnov, H. Motzkau, T. Golod, A. Rydh, S. O. Katterwe, and A. B. Kulakov, Comparative analysis of tunneling magnetoresistance in low- T_c Nb/Al-AlO_x/Nb and high- T_c Bi_{2-y}Pb_ySr₂CaCu₂O_{8+δ} intrinsic Josephson junctions, *Phys. Rev. B* **84**, 054516 (2011).
- [17] D. V. Evtushinsky, V. B. Zabolotnyy, L. Harnagea, A. N. Yaresko, S. Thirupathaiah, A. A. Kordyuk, J. Maletz, S. Aswartham, S. Wurmehl, E. Rienks, R. Follath, B. Büchner, and S. V. Borisenko, Electronic band structure and momentum dependence of the superconducting gap in Ca_{1-x}Na_xFe₂As₂ from angle-resolved photoemission spectroscopy, *Phys. Rev. B* **87**, 094501 (2013).
- [18] P. Szabó, Z. Pribulová, G. Pristáš, S. L. Bud'ko, P. C. Canfield, and P. Samuely, Evidence for two-gap superconductivity in Ba_{0.55}K_{0.45}Fe₂As₂ from directional point-contact Andreev-reflection spectroscopy, *Phys. Rev. B* **79**, 012503 (2009).
- [19] D Daghero, M Tortello, G A Ummarino and R S Gonnelli, Directional point-contact Andreev-reflection spectroscopy of Fe-based superconductors: Fermi surface topology, gap symmetry, and electron-boson interaction, *Rep. Prog. Phys.* **74**, 124509 (2011).
- [20] Yu. G. Naidyuk, O. E. Kvitnitskaya, S. Aswartham, G. Fuchs, K. Nenkov, and S. Wurmehl, Exploring point-contact spectra of Ba_{1-x}Na_xFe₂As₂ in the normal and superconducting states, *Phys. Rev. B* **89**, 104512 (2014).
- [21] S. Ziemak, K. Kirshenbaum, S. R. Saha, R. Hu, J.-Ph. Reid, R. Gordon, L. Taillefer, D. Evtushinsky, S. Thirupathaiah, B. Büchner, S. V. Borisenko, A. Ignatov, D. Kolchmeyer, G. Blumberg and J. Paglione, Isotropic multi-gap superconductivity in BaFe_{1.9}Pt_{0.1}As₂ from thermal transport and spectroscopic measurements, *Supercond. Sci. Technol.* **28**, 014004 (2015).
- [22] Y. F. Wu, A. B. Yu, L. B. Lei, C. Zhang, T. Wang, Y. H. Ma, Z. Huang, L. X. Chen, Y. S. Liu, C. M. Schneider, G. Mu, H. Xiao, and T. Hu, Superconducting NbN and CaFe_{0.88}Co_{0.12}AsF studied by point-contact spectroscopy with a nanoparticle Au array, *Phys. Rev. B* **101**, 174502 (2020).
- [23] A. A. Kalenyuk, A. Pagliero, E. A. Borodianskyi, S. Aswartham, S. Wurmehl, B. Büchner, D. A. Chareev, A. A. Kordyuk, and V. M. Krasnov, Unusual two-dimensional behavior of iron-based superconductors with low anisotropy, *Phys. Rev. B* **96**, 134512 (2017).
- [24] A. A. Kalenyuk, A. Pagliero, E. A. Borodianskyi, A. A. Kordyuk, and V. M. Krasnov, Phase-Sensitive Evidence for the Sign-Reversal s_{\pm} Symmetry of the Order Parameter in an Iron-Pnictide Superconductor Using Nb/Ba_{1-x}Na_xFe₂As₂ Josephson Junctions, *Phys. Rev. Lett.* **120**, 067001 (2018).
- [25] Y. Liu, M. A. Tanatar, W. E. Straszheim, B. Jensen, K. W. Dennis, R. W. McCallum, V. G. Kogan, R. Prozorov, and T. A. Lograsso, Comprehensive scenario for single-crystal growth and doping dependence of resistivity and anisotropic upper critical fields in (Ba_{1-x}K_x)Fe₂As₂ ($0.22 \leq x \leq 1$), *Phys. Rev. B* **89**, 134504 (2014).
- [26] A. Zeinali, T. Golod, and V. M. Krasnov, Surface superconductivity as the primary cause of broadening of superconducting transition in Nb films at high magnetic fields, *Phys. Rev. B* **94**, 214506 (2016).
- [27] S. O. Katterwe, A. Rydh, and V. M. Krasnov, Doping-Induced Change in the Interlayer Transport Mechanism of Bi₂Sr₂CaCu₂O_{8+δ} near the Superconducting Transition Temperature, *Phys. Rev. Lett.* **101**, 087003 (2008).
- [28] A. A. Golubov, M. Yu. Kupriyanov, and E. Il'ichev, The current-phase relation in Josephson junctions, *Review of Modern Physics* **76**, 411-469 (2004).
- [29] V. M. Krasnov, N. F. Pedersen, V. A. Oboznov, and V. V. Ryazanov, Josephson properties of Nb/Cu multilayers, *Phys. Rev. B* **49**, 12969 (1994).
- [30] V.M. Krasnov, V.A. Oboznov and V.V. Ryazanov, Anomalous temperature dependence of H_{c1}^{\perp} in superconducting Nb/Cu multilayer, *Physica C* **196**, 335-339 (1992).
- [31] A. A. Golubov, E.P. Houwman, J. G. Gijsbertsen, V. M. Krasnov, J. Flokstra, and H. Rogalla, Proximity effect in superconductor-insulator-superconductor Josephson tunnel junctions: Theory and experiment, *Phys. Rev. B* **51**, 1073 (1995).
- [32] <http://www.phys.ufl.edu/fermisurface/>
- [33] T.-S. Choy, J. Naset, J. Chen, S. Hershfield, and C. Stanton. A database of fermi surface in virtual reality modeling language (vrml). *Bulletin of The American Physical Society* **45**, L36.042 (2000).
- [34] A.N. Yaresko. Privat communication.
- [35] V. B. Zabolotnyy, D. S. Inosov, D. V. Evtushinsky, A. Koitzsch, A. A. Kordyuk, G. L. Sun, J. T. Park, D. Haug, V. Hinkov, A. V. Boris, C. T. Lin, M. Knupfer, A. N. Yaresko, B. Büchner, A. Varykhalov, R. Follath, and S. V. Borisenko, (π, π) electronic order in iron arsenide superconductors, *Nature* **457**, 569 (2009).
- [36] A. A. Kordyuk, V. B. Zabolotnyy, D. V. Evtushinsky, A. N. Yaresko, B. Büchner, S. V. Borisenko. Electronic band structure of ferro-pnictide superconductors from ARPES experiment. *J. Supercond. Nov. Magn.* **26**, 2837 (2013).
- [37] S. Schmidt, S. Döring, N. Hasan, F. Schmidl, V. Tympep, F. Kurth, K. Iida, H. Ikuta, T. Wolf, and P. Seidel, Josephson effects at iron pnictide superconductors: Approaching phase-sensitive experiments, *Phys. Stat. Sol. B* **254**, 1600165 (2017).